PNAS
www.pnas.org

Supplementary Information for

Title: Climate-driven variation in mosquito density predicts the spatio-temporal dynamics of dengue

Authors: Ruiyun Li, Lei Xu, Ottar N. Bjørnstad, Keke Liu, Tie Song, Aifang Chen, Bing Xu, Qiyong Liu and Nils C. Stenseth

This PDF file includes:

Figs. S1 to S9
Tables S1 to S3

www.pnas.org/cgi/doi/10.1073/pnas.1806094116

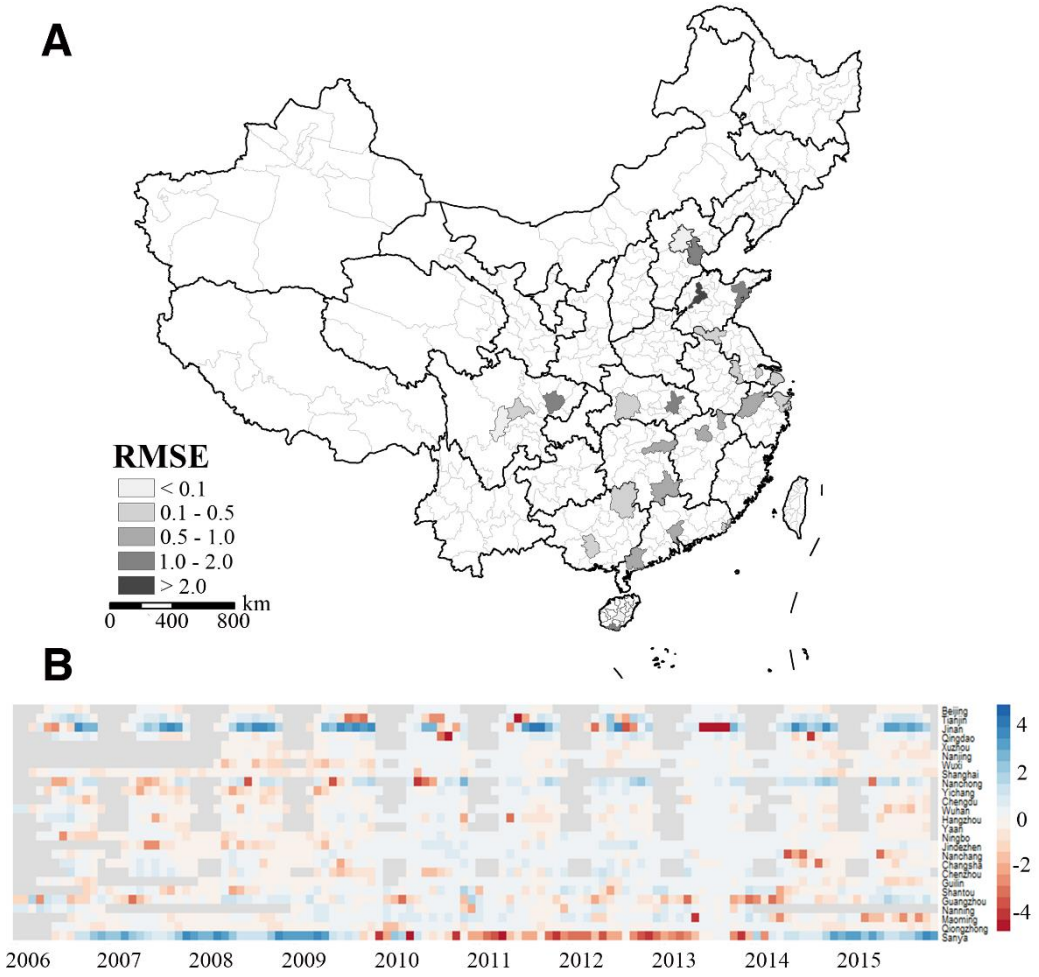

Fig. S1. The accuracy of mosquito estimates in 26 cities. (A) The root-mean-square error (RMSE) of the estimated mosquito density in 2006-2015 and (B) the corresponding variation in each month are used to quantify the accuracy of statistical analysis in each city.

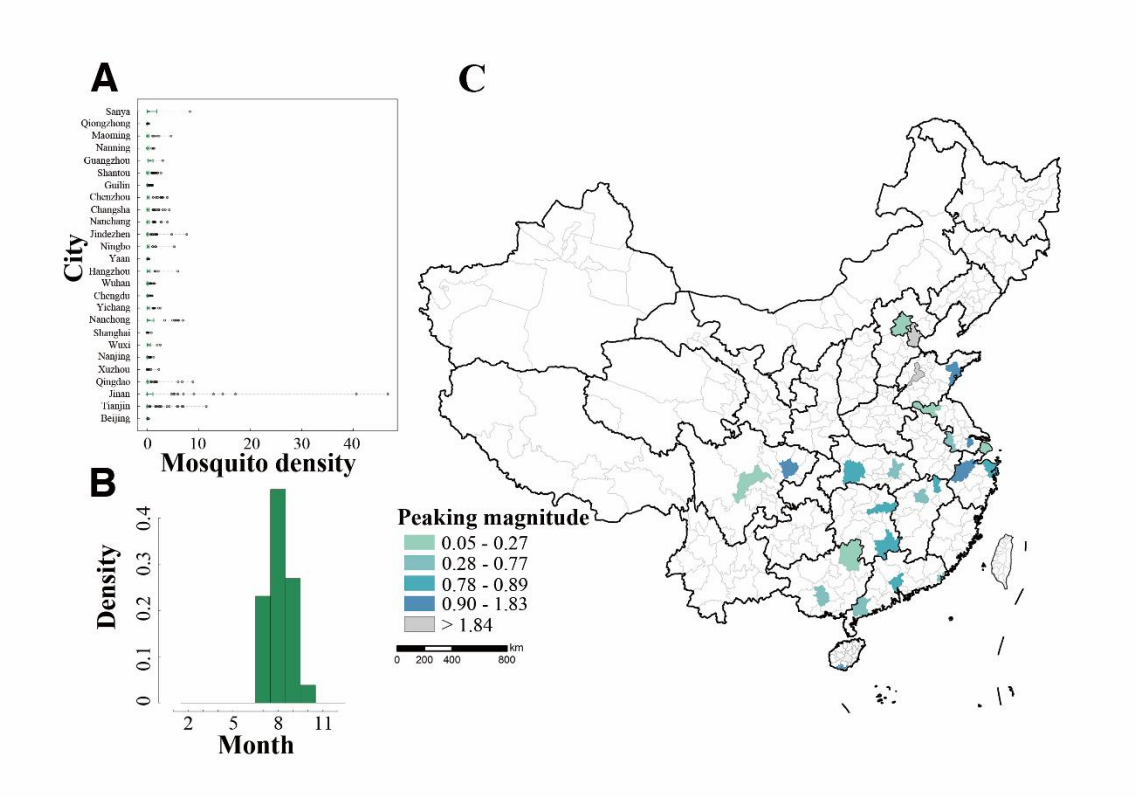

Fig. S2. Spatial-temporal distribution of mosquito density in 26 cities. (A) the interquartile range (IQR) and outliers of the observed mosquito density in each city is indicated by green bars and black dots, respectively. City is aligned from North to South according to their latitude. (B) The distribution of peak timing, i.e., the month with the largest mosquito abundance, of the estimated mosquito density in 26 cities in 2005-2015 is used to reflect the seasonality of mosquito population. (C) The spatial distribution of peaking magnitude, i.e., the annual largest mosquito abundance, is colored based on the relative abundance across cities.

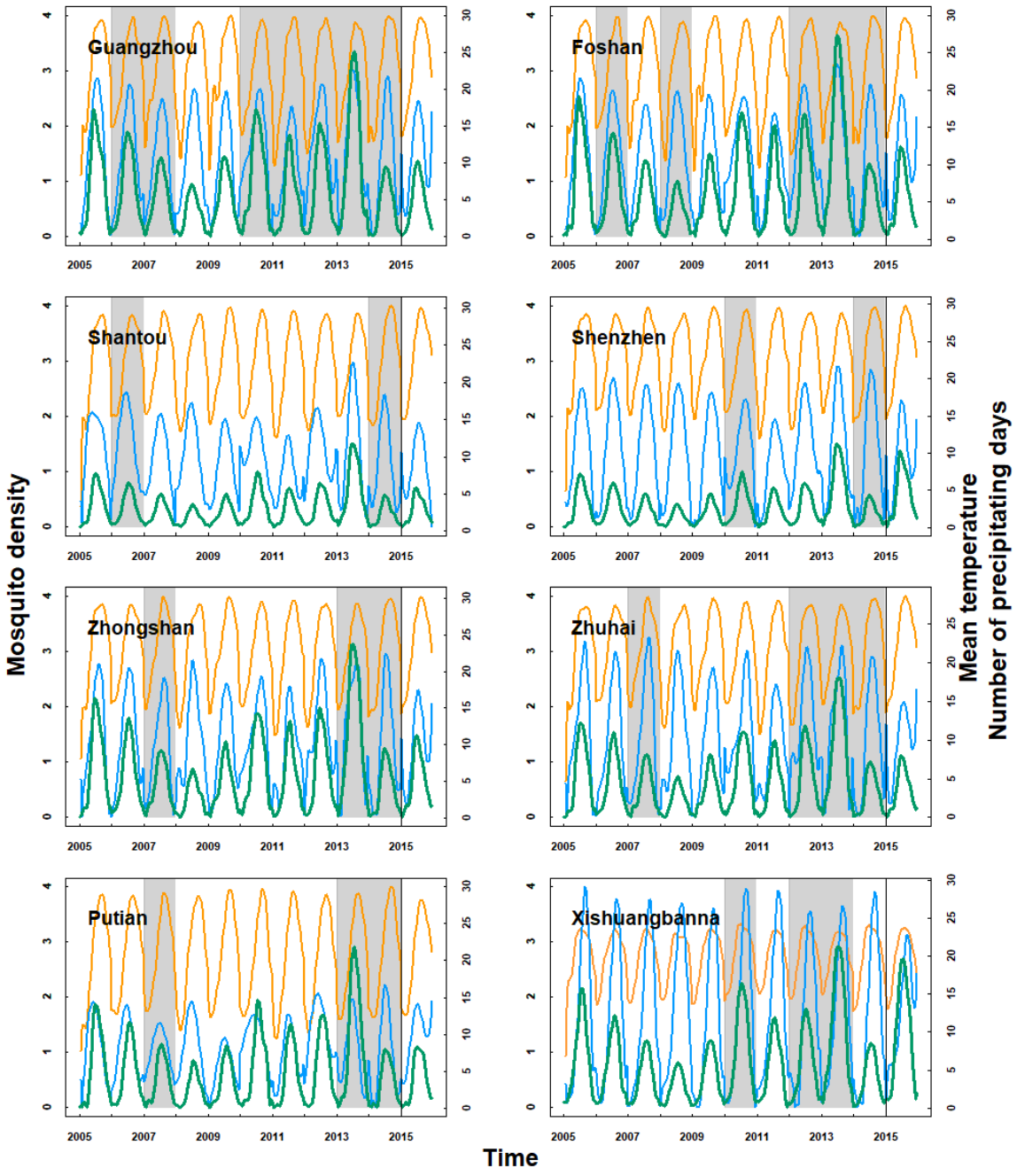

Fig. S3. The times series of the estimates of mosquito density and corresponding meteorological conditions in the 8 training cities for SIR model. The mosquito density (green lines) reconstructed by local mean temperature (yellow lines) and number of precipitating days (blue lines) in outbreak years (grey shaded area) in 2005-2014 are used for mathematical simulation and parameter estimation; while those in 2015 are employed for the forecast of dengue human infections.

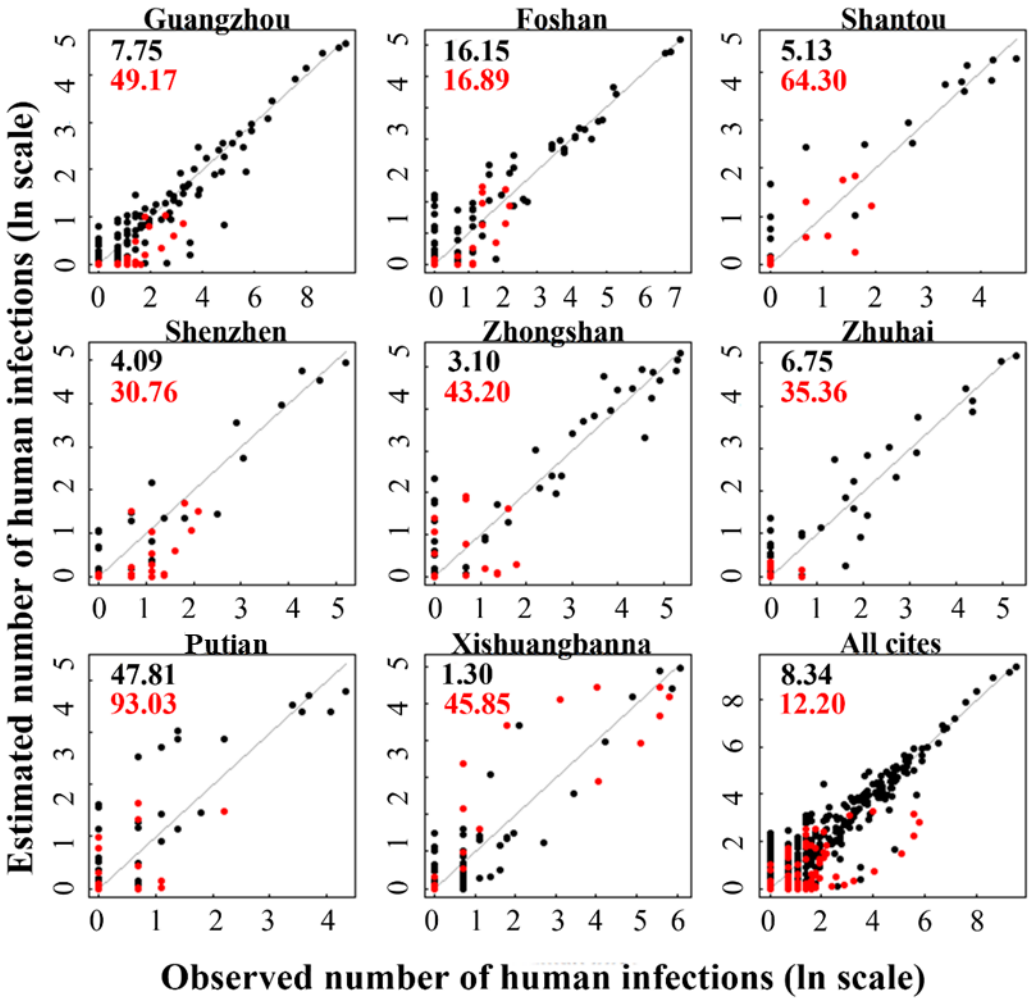

Fig. S4. The accuracy of the inference of human infections in 2005-2015. The observed and estimated magnitude of human infections in the simulation (i.e., 2005-2014) and prediction (i.e., 2015) period is plotted on the logarithmic scale using black and red dots, respectively. The corresponding quantitative assessment of accuracy is made using RMSE.

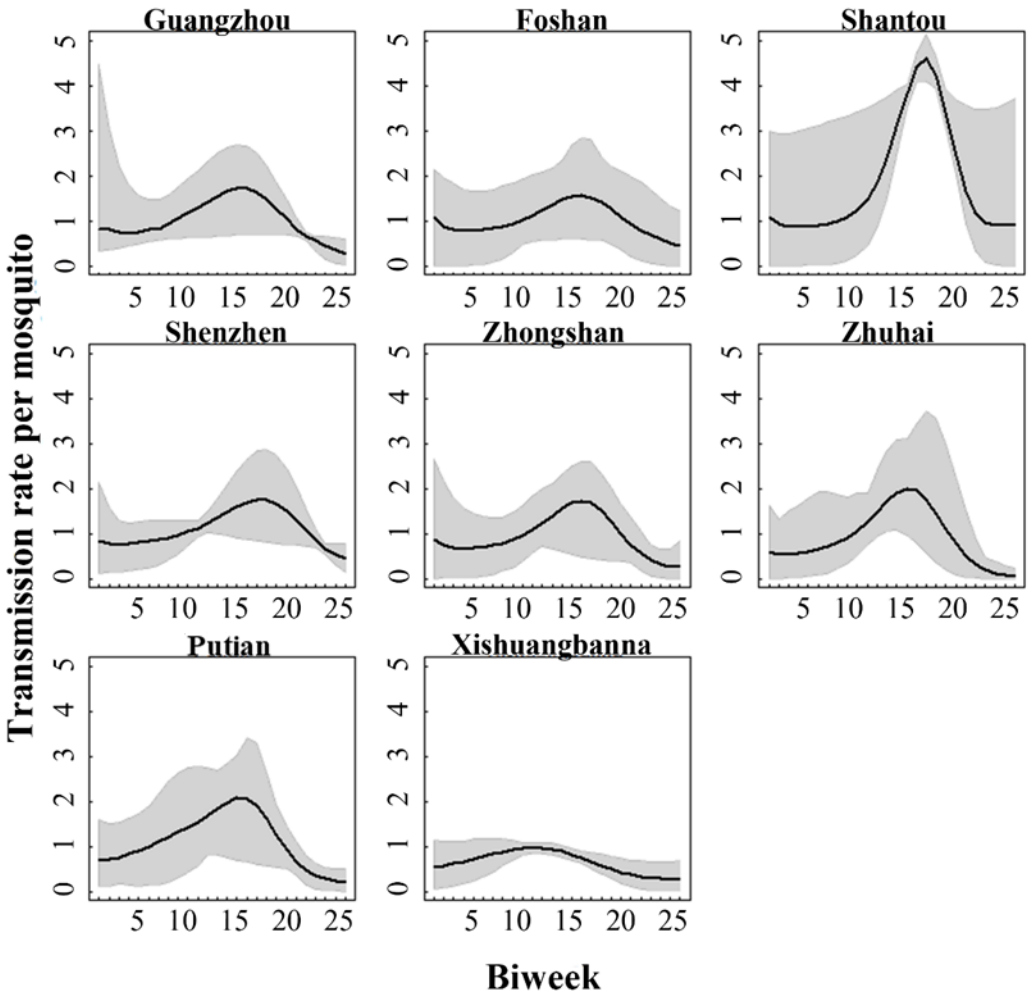

Fig. S5. The inferred dynamic pattern of per mosquito vector efficiency. The median estimates (black lines) and the corresponding 5th and 95th quantile interval (grey shaded area) represent the seasonality of $\beta'(t)$ in each city in 2005-2014.

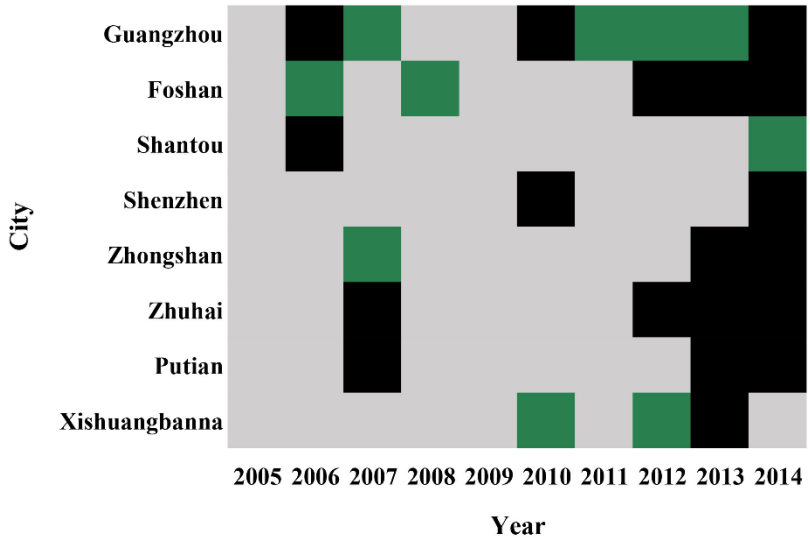

Fig. S6. The dominant factor of transmission risk across outbreak years and cities. The inferred dominance of mosquito abundance (green) *versus* vector efficiency (black) in regulating transmission risk among humans in outbreak years. Non-outbreak years are excluded in the analysis (grey shaded area).

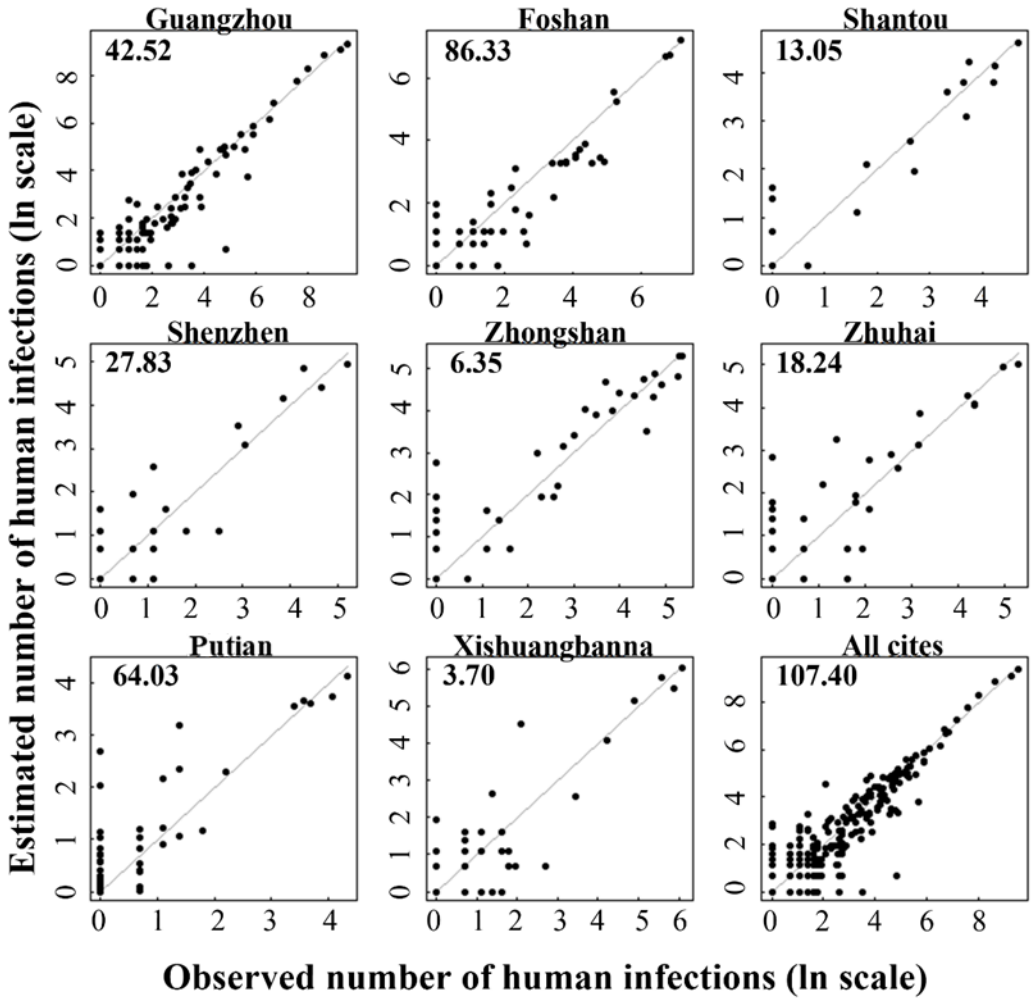

Fig. S7. The accuracy of the inference of human infections in 2005-2014 using the null model. The null model without the incorporation of mosquito abundance in transmission rate was used to infer human infections of outbreak years in 2005-2014. The observed and estimated magnitude of human infections is plotted on the logarithmic scale. The corresponding quantitative assessment of accuracy is made by RMSE.

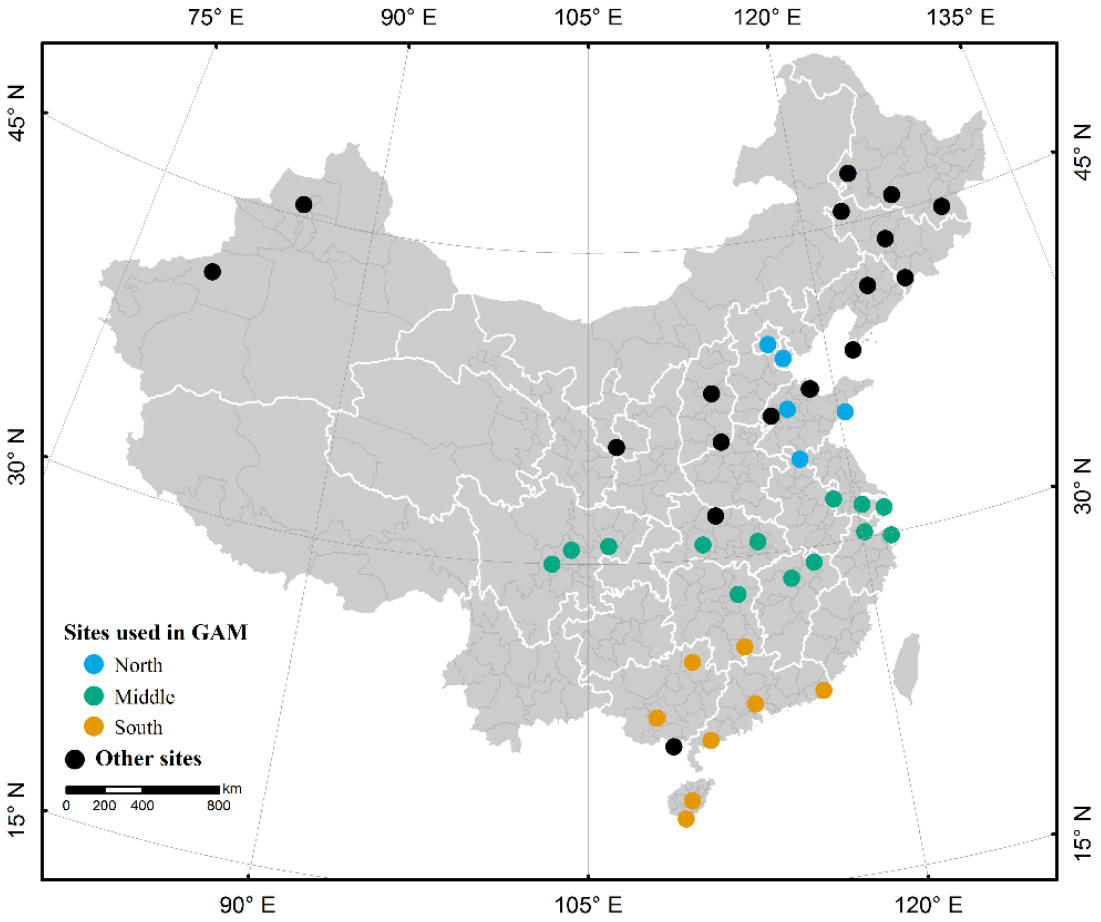

Fig. S8. Distribution of mosquito surveillance sites. Mosquito surveillance of 26 sites located in North (blue), Middle (green) and South (yellow) area is used for the analysis of weather-abundance associations. The observed mosquito density of the other 18 sites (black) is zero in 2005-2015, and thus are excluded in the statistical analysis.

Fig. S9. Distribution of the eight cities used to parameterize the SIR model. Cities with distinct outbreak years (i.e., year with prominent incidence of human infections) during 2005-2014 were selected for mathematical model simulation and parameter estimation. Additionally, human infections in 2015 in these cities were predicted as an out-of-sample validation of our model.

Table S1. Performance of statistical model in fitting the mosquito abundance in 26 surveillance sites in 2006-2015. The performance of model with no, one-month and two-month lag between local weather conditions and mosquito abundance is quantified by the generalized cross-validation criterion (GCV), the proportion of deviation explained by model and the significant weather predictors ($p < 0.05$).

Model	Model formula	GCV	Deviance explained (%)	Significant weather predictors
Zero lag	$M_{i,j} = a_{i,j} + b(Lon_j, Lat_j) + c(T_{i,j}) + d(P_{i,j}*Area) + \varepsilon_{i,j}$	1914.83	42.6	$T_{i,j}$
One-month lag	$M_{i,j} = a_{i,j} + b(Lon_j, Lat_j) + c(T_{i-1,j}) + d(P_{i-1,j}*Area) + \varepsilon_{i,j}$	1888.16	42.8	$T_{i-1,j}$ $P_{i-1,j}$ in each area
Two-month lag	$M_{i,j} = a_{i,j} + b(Lon_j, Lat_j) + e(T_{i-2,j}) + f(P_{i-2,j}*Area) + \varepsilon_{i,j}$	2016.20	35.5	$T_{i-2,j}$ $P_{i-2,j}$ in each area

Table S2. SIR model performance using time-dependent and constant per mosquito vector efficiency. To evaluate model performance with time-dependent $\beta'(t)$ against the constant β', likelihood ratio test was implemented across cities and years using test statistic (T) with the following form: T = -2 * (log-likelihood for model with $\beta'(t)$ – log-likelihood for model with β').

City	Year	Log-likelihood for model		Likelihood ratio test
		$\beta'(t)$	β'	T
Guangzhou	2006	197.48	29904.76	59414.56*
	2007	28.31	35.44	14.26*
	2010	42.46	165.81	246.70*
	2011	65.49	140.06	149.14*
	2012	50.30	119.54	138.48*
	2013	234.78	131643.80	262818.00*
	2014	1919.18	78700931.32	15700000.00*
Foshan	2006	12.83	115.70	205.74*
	2008	35.02	100.87	131.70*
	2012	84.64	2196.23	4223.18*
	2013	38.16	3534.59	6992.86*
	2014	105.27	738436.00	1476661.00*
Shantou	2006	100.38	3714.65	7228.54*
	2014	67.29	1719.68	3304.78*
Shenzhen	2010	31.76	68.82	74.12*
	2014	67.09	7090.45	14046.72*
Zhongshan	2007	16.32	83.10	133.56*
	2013	196.81	11037.83	21682.04*
	2014	39.89	13993.95	27908.12*
Zhuhai	2007	45.73	2815.48	5539.50*
	2012	18.15	40.28	44.26*
	2013	25.29	123.41	196.24*
	2014	43.89	11213.74	22339.50*
Putian	2007	30.80	1866.94	3672.28*
	2013	28.16	31.69	7.06
	2014	21.92	2151.89	4259.94*
Xishuangbanna	2010	19.80	36.22	32.84*
	2012	37.62	41.03	6.82
	2013	180.24	151146.95	301933.40*

*statistical significance ($p < 0.05$).

Table S3. The relative proportion of *A. Albopictus* and *A. Aegypti* species in the 26 cities in 2005-2015. The composition of dengue-related mosquito population in each city is reflected by the relative proportion of two mosquito species.

City	Proportion (%)		City	Proportion (%)	
	A. Albopictus	*A. Aegypti*		*A. Albopictus*	*A. Aegypti*
Beijing	100	0	Chengdu	100	0
Xuzhou	100	0	Nanchong	100	0
Jinan	100	0	Yaan	100	0
Qingdao	100	0	Ningbo	100	0
Tianjin	100	0	Hangzhou	100	0
Wuhan	100	0	Guangzhou	100	0
Yichang	100	0	Maoming	96.1	3.9
Changsha	100	0	Shantou	100	0
Wuxi	100	0	Guilin	100	0
Nanjing	100	0	Nanning	100	0
Jindezhen	100	0	Qiongzhong	100	0
Nanchang	100	0	Sanya	95.49	4.51
Shanghai	100	0	Chenzhou	100	0